Hindawi
Geofluids
Volume 2023, Article ID 7979348, 12 pages
https://doi.org/10.1155/2023/7979348

Research Article

A Three-Dimensional Display Technology of Reflected Acoustic Logging and Its Application Example

Li Dan

Cnooc Research Institute Ltd., Beijing 100028, China

Correspondence should be addressed to Li Dan; lidan6@cnooc.com.cn

Received 23 October 2022; Revised 9 December 2022; Accepted 20 March 2023; Published 15 April 2023

Academic Editor: Peng Tan

Reflection acoustic logging is a new technology for identifying geological structures around the well. It can be used to describe the geological structure, such as formation interface, fracture, and limestone cave. Based on the acoustic logging tool composed of the source and array receiver, the method can be used to image the geological structure around the well. Through migration imaging, the section crossing the well can be obtained in any azimuth. In the current three-dimensional (3D) display technology of reflection acoustic logging, the reflection plane around the well is always displayed as a reflection arc. The arc surface correction method can correct the arc surface in 3D imaging into a plane. According to the similarity criterion in a physical experiment and the need for practical research, we designed a scale model well experiment of dipole reflection acoustic logging. We obtained the 3D display of the reflection structure around the well by the experiment and realized the arc surface correction of the 3D display in reflection acoustic logging. The application shows the method can qualitatively describe the lateral extension length of the geological structure around the well. After the arc surface correction, the geological structure can be more accurately described.

1. Introduction

Reflection acoustic logging is a new well-logging technology, which is concerned researched widely in recent years [1–10]. This method can be used to identify the geological structure and evaluate the fracturing effect in unconventional oil and gas exploration [11–17]. The resolution of reflected acoustic logging is near 20 cm, which is better than that of seismic exploration. The detection depth is nearly 50 meters, which is much greater than that of conventional acoustic logging. Schlumberger company first introduced the prototype of the borehole acoustic reflection survey (BARS) in 1998 [18]. The previous reflected P-wave imaging logging used a monopole source and receiver. The results can only judge the distance from the structure to the borehole and cannot explain its azimuth [19]. In order to overcome the shortcomings of the monopole P-wave method, Tang et al. introduced the dipole S-wave reflection acoustic logging technology, which used a dipole source and dipole receiver in reflection acoustic logging [20–23]. This method uses the orthogonal dipole source to radiate the shear wave to the formation outside the well and receives the shear wave reflected from the formation to image the structure near the borehole. Through wavefield separation, synthesis of reflected SH-wave, and migration imaging, the image of any azimuth section through the borehole can be obtained. By comparing them, the trend of the reflector can be judged. With the improvement of geologists' requirements for the display, more and more researchers use 3D space to display the reflectors near the borehole. Li Chao processed the logging data of monopole reflection acoustic logging and obtained the 3D display of the reflector near the borehole by using the scattered map [24]. Li and Yue used two imaging sections with different azimuths to form a 3D display and gave the top view of one depth point [25, 26]. Kumar et al. used the 3D-STC method and ray tracing method to process and analyze the

logging data of Sonic Scanner. Since this method does not adopt migration imaging, this method only displays multiple slice results in the 3D window [27]. The inclination and azimuth of the reflector near the borehole can be obtained from the slicing results, but there is no direct image of the geological structure. Yevgeniy et al. combined the 2D imaging with the geological model into 3D graphics for display. This method displays the logging processing software data and geological model data in the same software for the first time [28]. The above methods all face a problem in 3D display results. When there is a reflection plane near the well, the 3D result is a reflection-curved surface.

This paper studies the method of curved surface correction in the 3D display of reflection acoustic logging, which can correct the arc surface to a plane in 3D imaging. According to the similarity criterion in the experiment and the need for practical research, the scale model well experiment of dipole reflection shear wave logging is designed. By processing the experimental data, the 3D display of the reflection plane is obtained, and the arc surface correction of the 3D display of the dipole reflection shear wave logging is finally realized. The arc surface correction technique is applied to process the actual logging data. The results show that this method can qualitatively describe the lateral extension length of the fracture near the borehole compared with the current 3D image display of reflection acoustic logging. After arc surface correction, the reflector near the borehole can be more accurately depicted.

2. Method

Dipole reflection shear wave logging can synthesize SH waves in any direction through four component waveforms.

$$\mathrm{SH}(\varphi) = \mathrm{XX}\sin^2\varphi + (\mathrm{XY} + \mathrm{YX})\sin\varphi\cos\varphi + \mathrm{YY}\cos^2\varphi, \tag{1}$$

where XX and XY, respectively, represent the waveforms emitted by the dipole X and received by the dipole X and Y receivers; YX and YY, respectively, represent the waveforms emitted by the dipole Y and received by the dipole X and Y receivers.φ is the angle of the tool azimuth from the well logging. There are two problems in the 3D display of dipole reflected shear wave: first, the actual reflection plane is displayed as a reflection arc. The other is that one actual reflection surface is displayed as two reflection surfaces, and the azimuth angle difference between the two reflecting surfaces is 180°. In order to obtain the 3D display of the reflection plane, it is necessary to correct the arc surface position of the imaging data that cannot be correctly returned. The specific steps are as follows:

(1) Through dipole reflection shear wave logging, 2D imaging section and reflection trends θ in different azimuths are obtained

(2) Take the top view of a reflection interface as an example. In Figure 1, point O is the center of the borehole. Point A is the top viewpoint (i.e. imaging data point) of the intersection of the section and the imaging reflection (arc surface). Point A` is the top viewpoint of the intersection of the section and the real reflection. Therefore, points A need to be corrected to points A`, and the position information of A and A` relative to the well axis needs to be calculated in the correction process. The coordinates of point A in the cylindrical coordinate system are A($\mathrm{R}, \theta + \Delta\theta, \mathrm{z}$). Where $\Delta\theta$ is the included angle between the orientation of the section and the orientation of the reflector. R is the distance from the reflector to the point O. The coordinates of the midpoint A in the rectangular coordinate system are A ($\mathrm{x_A}, \mathrm{y_A}, \mathrm{z}$). Where $\mathrm{x_A}, \mathrm{y_A}, \mathrm{z}$ are, respectively

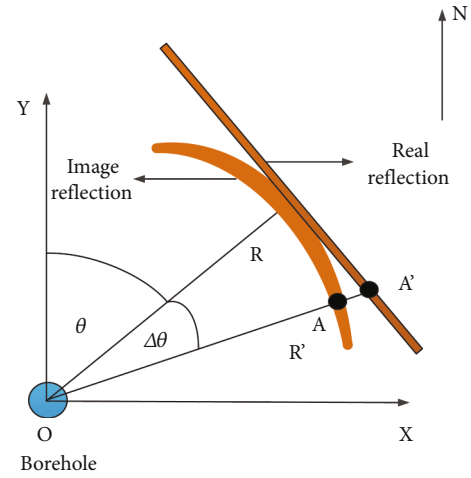

Figure 1: Schematic diagram of curved surface correction.

$$\begin{aligned} \mathrm{x}_A &= R \times \sin(\theta + \Delta\theta), \\ \mathrm{y}_A &= R \times \cos(\theta + \Delta\theta). \end{aligned} \tag{2}$$

The coordinates of the point A` in the cylindrical coordinate system should be A`($\mathrm{R}`, \theta + \Delta\theta, \mathrm{z}$). The coordinates of the point A` in the Cartesian coordinate system shall be A`($\mathrm{x_{A`}}, \mathrm{y_{A`}}, \mathrm{z}$). Where $\mathrm{x_{A`}}, \mathrm{y_{A`}}, \mathrm{z}$ are, respectively,

$$\begin{aligned} R' &= R \div \cos(\Delta\theta), \\ \mathrm{x}_{A'} &= R \div \cos(\Delta\theta) \times \sin(\theta + \Delta\theta), \\ \mathrm{y}_{A'} &= R \div \cos(\Delta\theta) \times \cos(\theta + \Delta\theta). \end{aligned} \tag{3}$$

Correct point A in space to point A` to complete the arc surface correction.

(3) Perform position correction on the imaging data of the reflection at all depth points. Return to the actual position, that is, completes the 3D correction. The 3D image after arc surface correction is displayed by top view, side view, and multiazimuth view and can also be displayed as a dynamic image

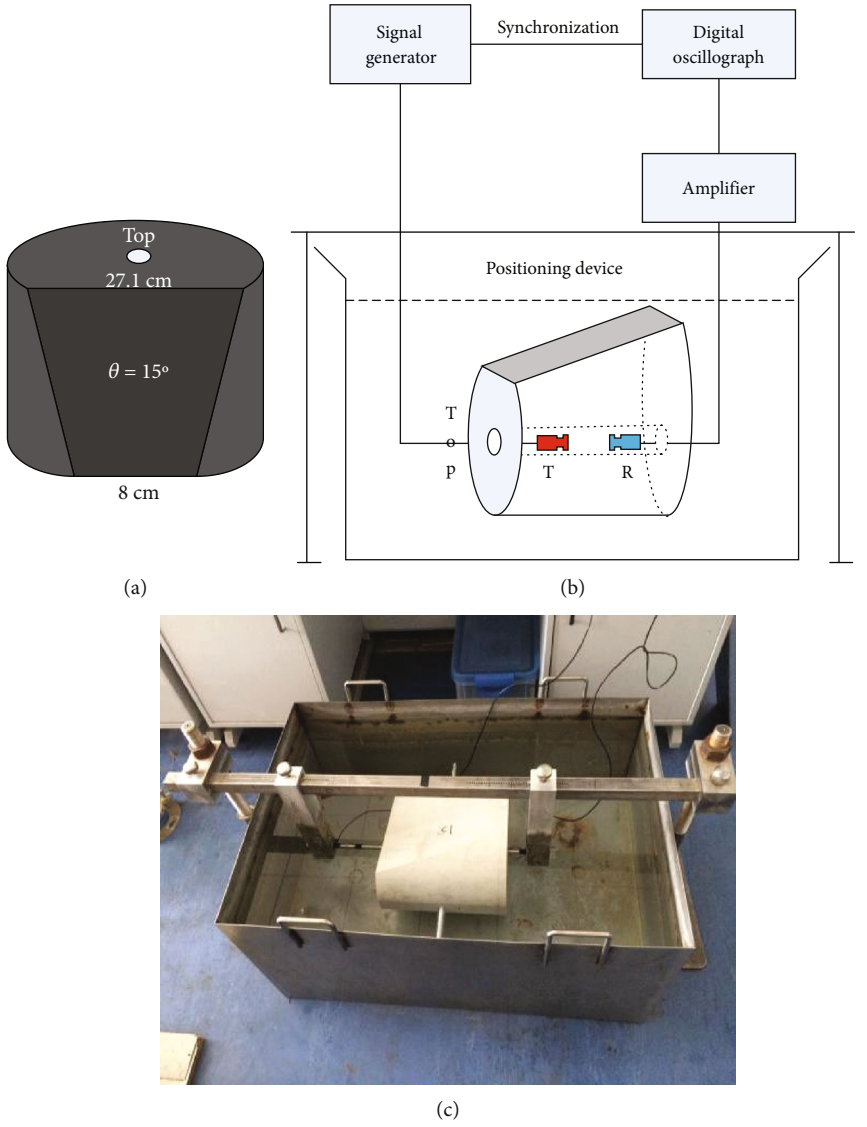

Figure 2: Physical photos and schematic diagram of the experimental device. (a) The scale model well with a reflection. (b) Schematic diagram of experimental device. (c) Physical drawing of the experimental device.

3. Experiment

3.1. Experiment Introduction. The experimental device is shown in Figure 2, mainly including a scale model well, dipole transmitting and receiving probe, water tank mechanical system, signal generator, and signal acquisition system. The scale model well has an outer diameter of 30 cm, a height of 30 cm, and a borehole diameter of 1.4 cm. The inclined surface on one side of the model well is taken as the reflection. The inclination of the reflection is 75°. The top distance of the reflection is 6.4 cm away from the borehole, and the bottom distance of the reflection is 14.5 cm. The material of the model well is a homopolymer, and the P-wave and S-wave velocities are 2300 M/s and 990 m/s, respectively. During the experiment, the model well was placed in a water tank, and the dipole transmitting and receiving probes were placed in the middle of the borehole. The main frequency of the excitation signal used in the experiment is 40 kHz.

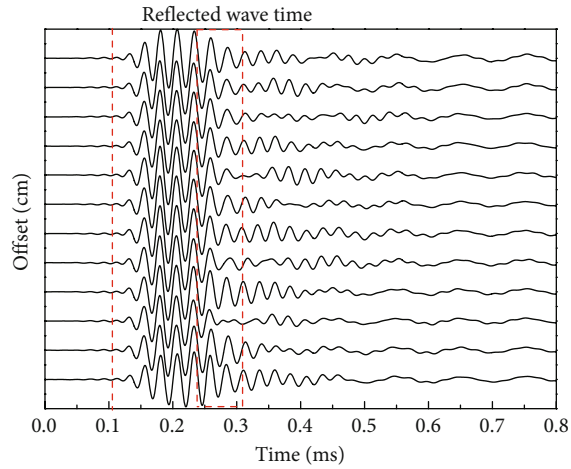

Figure 3: The YY waveform of common offset gather in 10 cm.

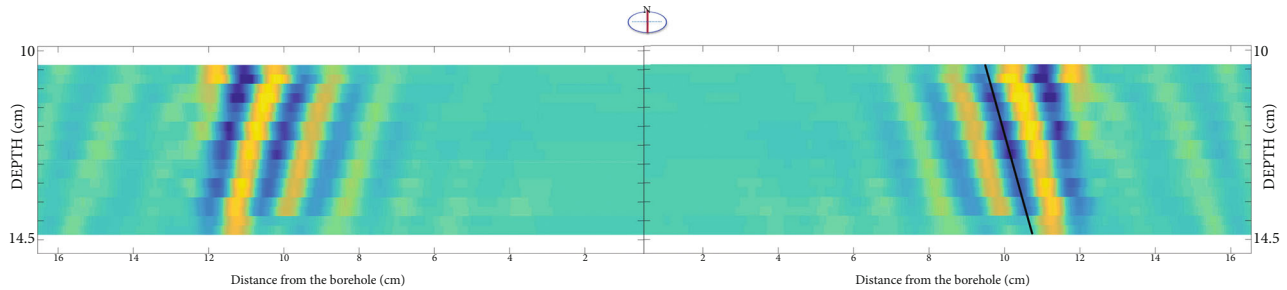

Figure 4: Migration imaging of north to south profiles.

The experimental process is as follows: the model well top is defined as the depth zero point, the midpoint of the transmitting and receiving probe is the depth recording point, and the reflection interface is located in the north direction. Define the north-south direction as the X direction, and define the East-West direction as the Y direction. At the initial moment, the depth recording point is 9 cm, that is; the depth of the dipole transmitting probe and the receiving probe is 4 cm and 14 cm, respectively.

(1) Set the dipole transmitting and receiving probe to be polarized along the X direction, and record a XX waveform. Keep the polarization direction of the transmitting probe unchanged, rotate the receiving probe so that the polarization direction of the receiving probe is polarized along the Y direction, and record an XY waveform. Keep the polarization direction of the receiving probe unchanged, rotate the transmitting probe to make the polarization direction of the transmitting probe polarized along the Y direction, and record a YY waveform. Keep the polarization direction of the transmitting probe unchanged, rotate the receiving probe so that the polarization direction of the receiving probe is polarized along the X direction, and record an YX waveform. At this time, we get a dipole four-component waveform at a depth point

(2) Continuously move the probe in steps of 0.5 cm. After each movement, repeat step 1 to obtain dipole four component waveforms at depth points of 9.5, 10.0, 10.5, 11.0, 11.5, 12.0, 12.5, 13.0, 13.5, 14.0, and 14.5 cm. That is, 12 depth points were measured in this experiment, and a total of 12* 4 dipole four component waveforms were obtained

4. Experimental Result

Figure 3 is the waveform diagram of the YY component with a distance of 10 cm measured in the experiment. Since the dipole Y polarization direction is parallel to the interface trend, the YY component can obtain a strong reflected SH wave at this time, which is conducive to dipole-reflected S-wave imaging. It can be seen from the figure that the dipole wave appears after 0.1 ms and the wave has a good consistency. The reflected wave appears between 0.24 ms and 0.3 ms, and it can be seen that the amplitude of each channel waveform has an obvious difference in this time period. However, it is impossible to observe directly the phase axis of the reflected wave. The noise signals after 0.3 ms may come from the upper and lower top-bottom interfaces of the model well.

The four component dipole waveforms obtained from the simulation experiments are processed by band-pass filtering, singular value decomposition (SVD) to separate the borehole mode wave and reflected wave field, FK filtering to separate the up and down traveling waves, and deconvolution of the backlog wavelet. Multidirectional SH wave can be synthesized by changing at 5° intervals according to formula (1). After pre-stack, Kirchhoff migration imaging with the same migration parameters, 36 section images of 0° to 175° can be obtained. Figure 4 is the N-S sections. The black solid line marks the actual position of the reflection in the model well. It can be seen that the amplitude and clarity of the imaging data of the interface are displayed. In Figure 4, the inverted inclination of the reflection in the imaging diagram is between 74°to 75°, and the difference from the actual interface inclination of 75° is less than 1°. The distance between the top of the reflection and the borehole is about 10 cm in the image, the distance between the bottom of the reflection and the well axis is about 11.5 cm in the image, and the fact distance is 9 cm and 10.5 cm, respectively. The difference between them is about 1 cm. Figures 5(a) and 5(b) are the comparison images of depth slices before and after arc surface correction of 13 cm depth recording points, respectively. Through comparison, it can be seen that through the arc surface correction method, the 3D displayed arc surface can be corrected into a plane. And this display result will not change the amplitude of the imaging data. Figures 5(c) and 5(d) are the comparisons of the true north views before and after arc surface correction. It can be seen from the comparison that the top imaging value is larger than the bottom imaging value because the top is close to the well axis. In the 3D imaging results, the top lateral extension of the reflection is greater than the bottom lateral extension, which is consistent with the actual model well shape. Figures 5(e) and 5(f) are the due east 30° plan views before and after arc surface correction. After the arc surface correction process, the reflector is corrected into a reflection plane in the 3D display. Therefore, this display method is more intuitive for describing the geological body near the well.

5. Application

Well T is located in the southeast of the Sulige gas field central area in Ordos Basin. The measured depth of reflection acoustic logging is 3277 m-3943 m. Figure 6 is the migration

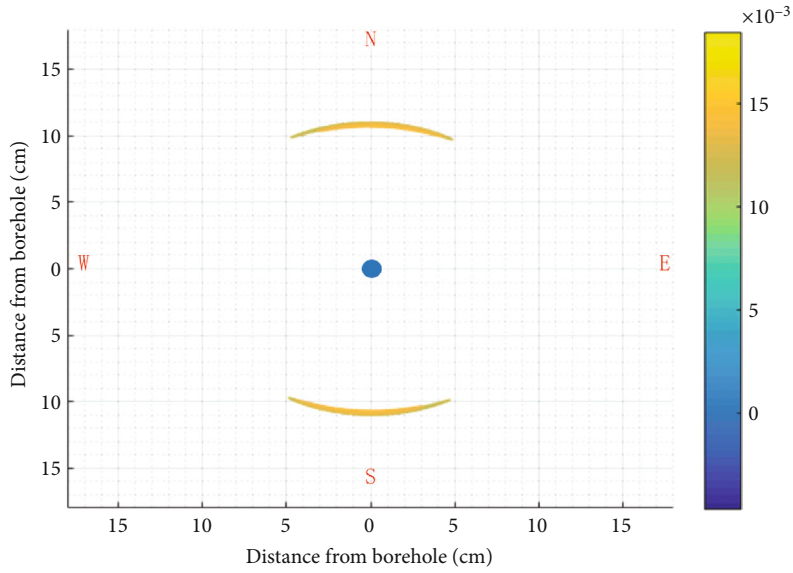

(a)

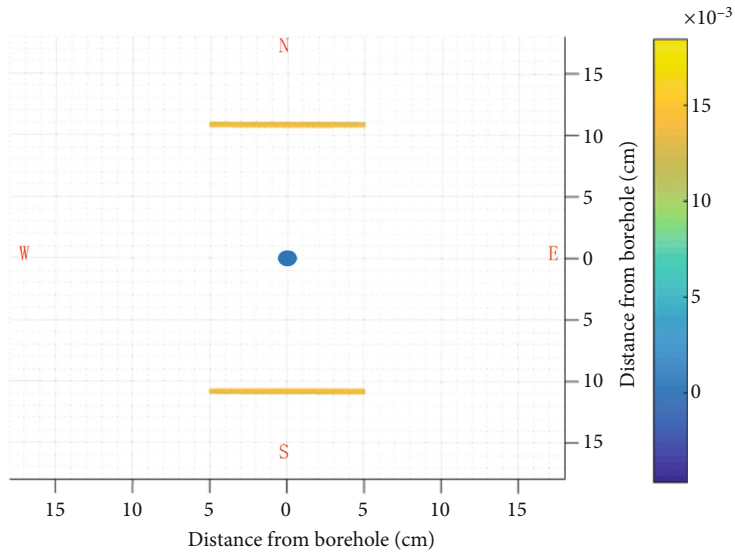

(b)

Figure 5: Continued.

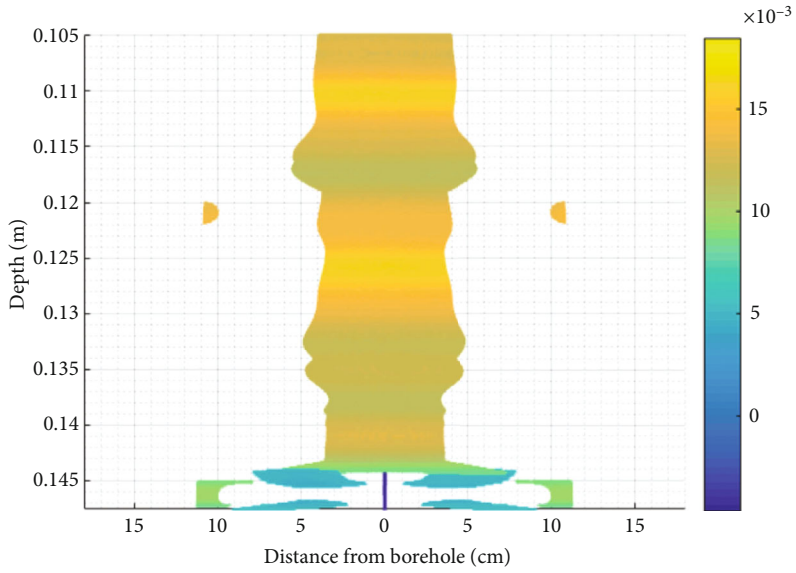

(c)

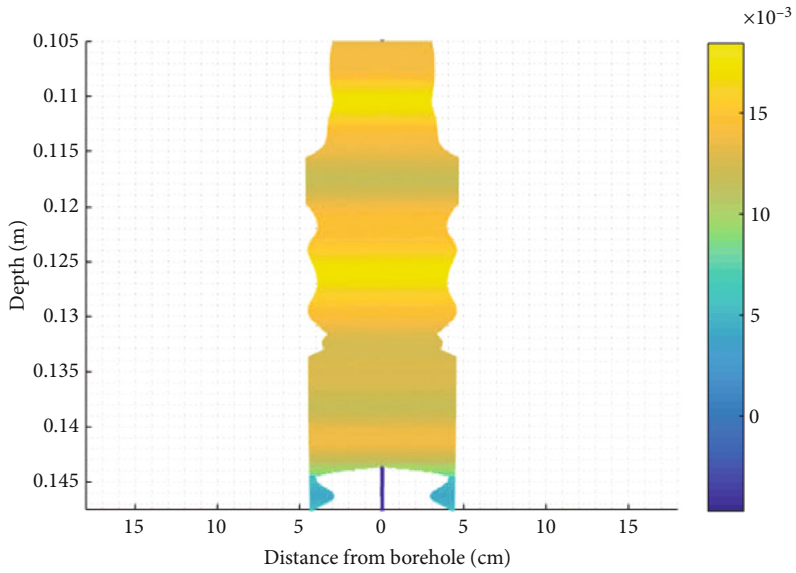

(d)

Figure 5: Continued.

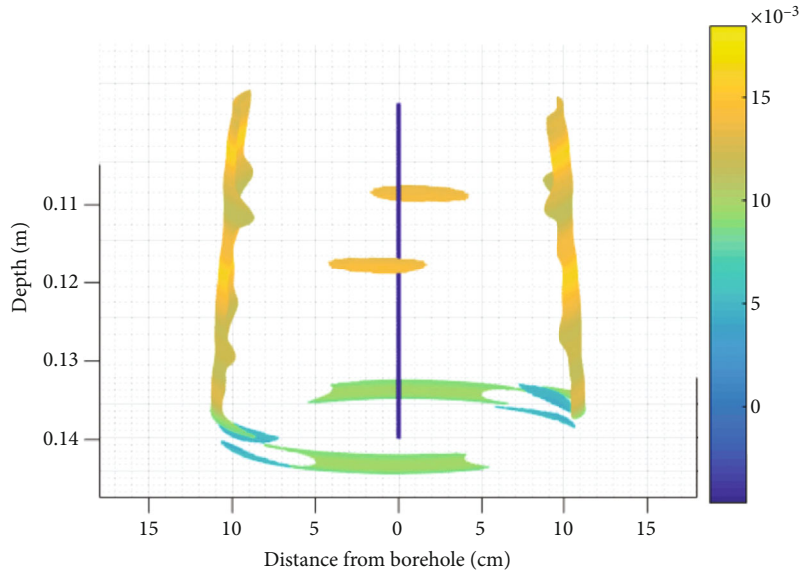

(e)

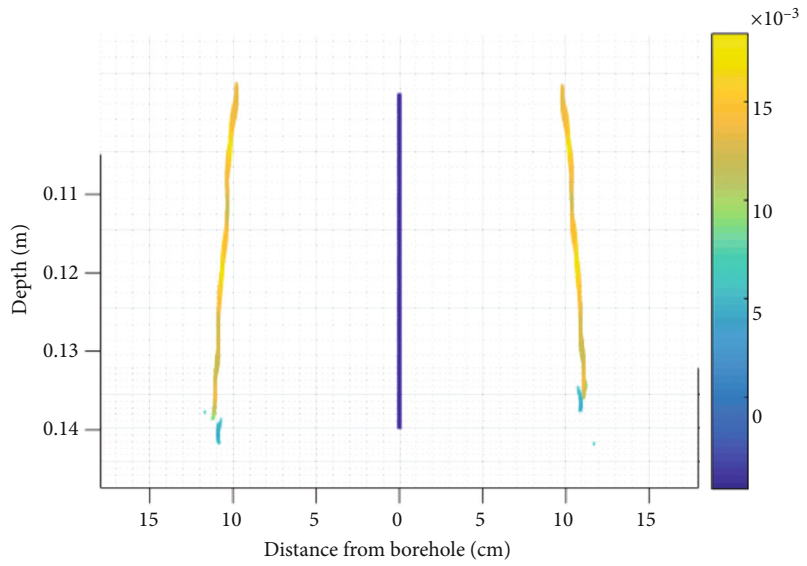

(f)

Figure 5: Three-dimensional display of model well experiment. (a) The section at a depth point of 13 cm. (b) The section at a depth point of 13 cm after the process. (c) Front view of the north. (d) Front north view of the north after the process. (e) The vertical view of 30°in the east. (f) The vertical view of 30°in the east after the process.

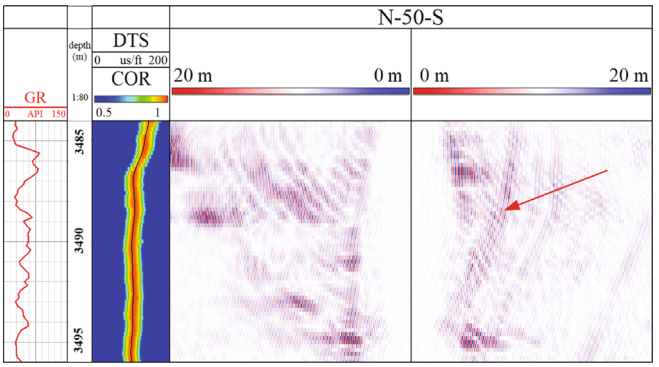

Figure 6: The profile migration imaging of north to south 50°.

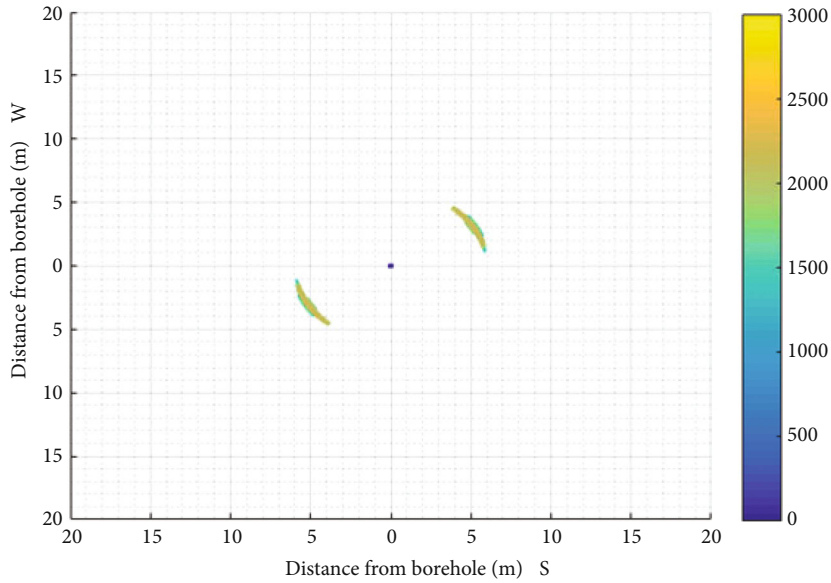

(a)

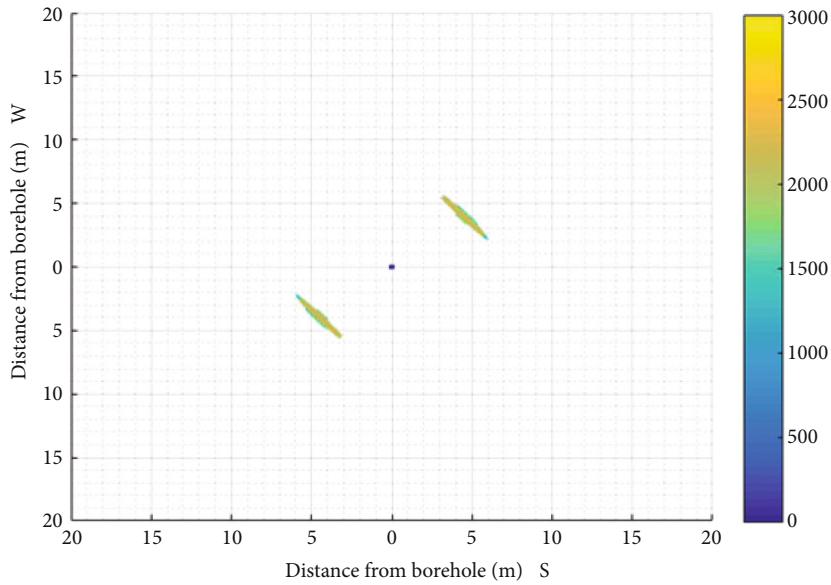

(b)

Figure 7: Continued.

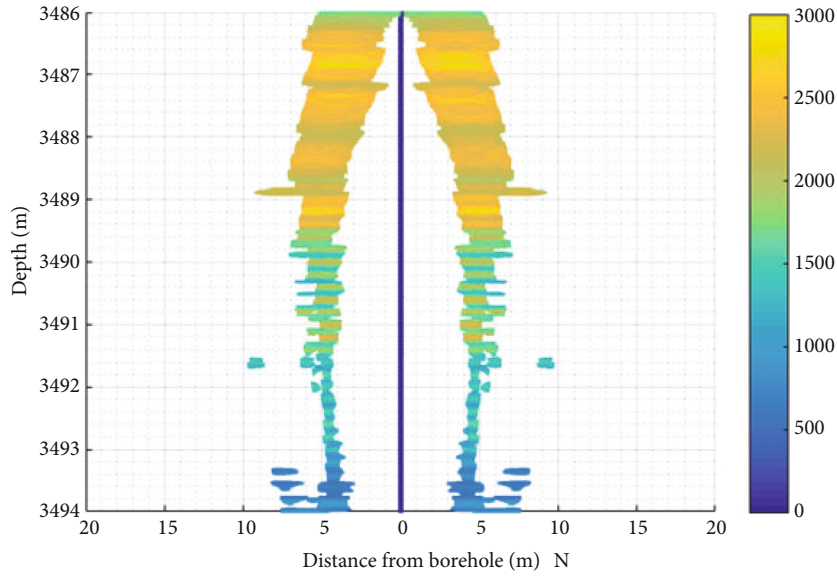

(c)

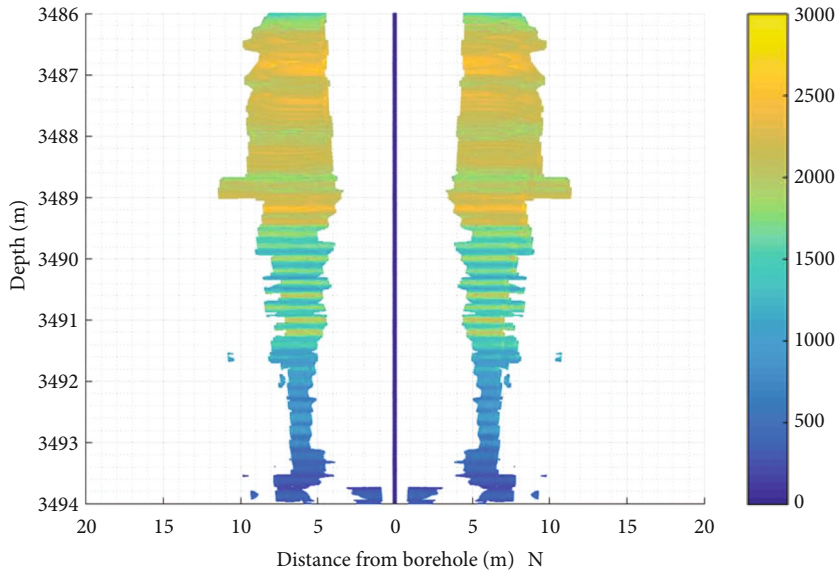

(d)

Figure 7: Continued.

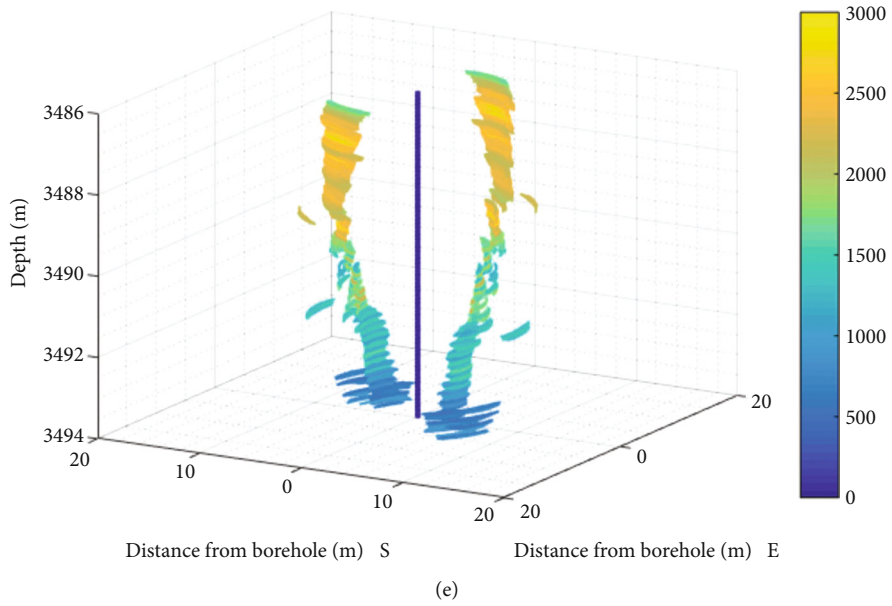

(e)

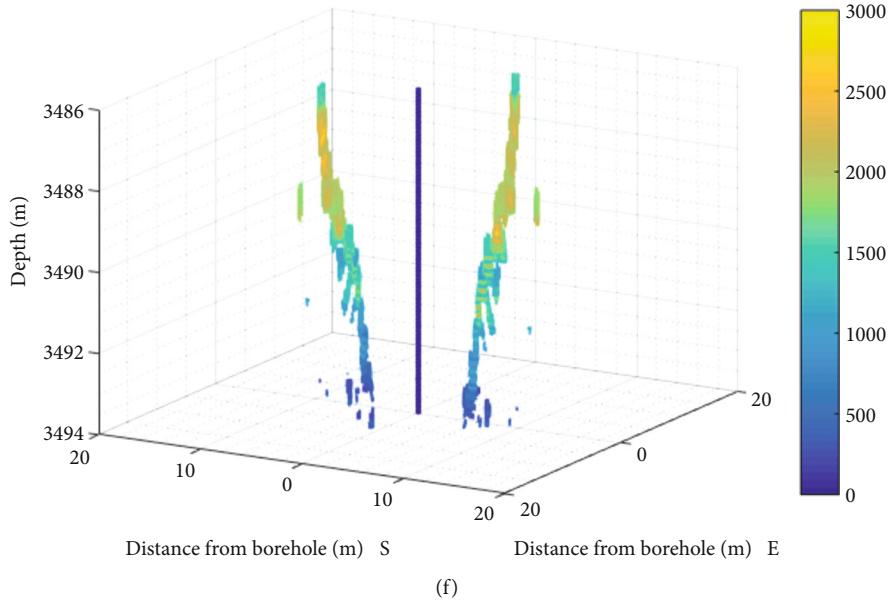

(f)

Figure 7: Three-dimensional display of fractures near the borehole by dipole reflection acoustic logging. (a) The section at a depth point of 3490 m. (b) The section at a depth point of 3490 m after the process. (c) Front view of the east. (d) Front north view of the east after the process. (e) The vertical view of 15°in the north to south 140°. (f) The vertical view of 15°in the north to south 140° after the process.

imaging result of the N-50-S section obtained from dipole reflection acoustic logging at 3485-3595 m depth. The first track is the GR curve, the second track is the depth track, and the third track is the S-wave velocity curve and correlation coefficient obtained after STC processing. The fourth track is the migration image of the cross-hole axis section. An inclined fracture (indicated by the red arrow) is shown in the depth section of 3486-3494 m. The total length of this fraction is 8 m, and the dip angle changes with the depth. The dip angle of the fractures in section 3486-3490 m is about 80°, and the dip angle of the fractures in section 3490-3494 m is about 70°. The upper end of the fracture is about 10 m away from the shaft, and the lower end is about 2 m away from the shaft. As shown in Figure 6, by comparing the amplitude of the multidirectional imaging data, it can be seen that the imaging characteristics of this fracture are the strongest in the N-50-S section. The arc surface correction method is applied to process the measured data. Figures 7(a) and 7(b) are the depth slice comparison of 3490 m depth without arc surface correction and after arc surface correction, respectively. Comparing the two figures, it can be seen that through the correction method in the paper, the well side arc surface display of a single depth point can be corrected to a plane display. Figures 7(c) and 7(d) are due east plan views before and after arc surface correction, respectively. By projecting the data of each depth into the 3D Cartesian coordinate system, the 3D display of the reflection beside the borehole can be obtained. Whether

surface correction arc is adopted or not, it can reflect the existence of this reflection interface. After the arc surface correction, the arc surface display of the geological body beside the well can be corrected into a plane display. Through 3D display and color code change, it can be observed that the fracture has a long transverse extension length and strong imaging amplitude at the depth of 3486-3489 m. At the depth of 3489-3494 m, the transverse extension length is short and the imaging amplitude is weak. Figures 7(e) and 7(f) are the 15° depression angle in the N50° direction before and after arc surface correction. The depression angle map in the 3D display is easier to express intuitively the orientation, shape, distance, and other characteristics of the geological body near the well and is also convenient for the observer to understand. After the arc surface correction, the reflector is corrected into a reflection plane in the 3D display.

6. Conclusion

Aiming at the problem of imaging surface in a 3D display of reflection acoustic logging, we propose a method of surface correction and apply it to physical experiments and field data. This method records multiple reflection imaging data points on the cross-section of different orientations. The data points are projected into the 3D Cartesian coordinate system by coordinate transformation, and the positions of the data points on the curved surface are corrected to obtain the reflection plane 3D map of the geological body near the well. The 3D display of the geological body near the well is carried out by using the physical experiment data and the field test data, and the following conclusions are obtained.

In the physical simulation experiment, the dip angle of the designed model well is 75°, and the azimuth is true north. In the migration imaging results, the dip angle of this reflection interface is 74°, and the azimuth is true north. The inversion error of the distance between the top and bottom ends of the interface and the well axis is less than 1 cm. After the arc surface correction, the reflection arc surface in the 3D display is corrected to a reflection plane, and the 3D display result of this reflection surface is basically consistent with the designed model well interface.

In the field data processing example, the fracture near the well is located at the n-50-s profile, and the distance between this reflector and the well axis is 2 m-10 m. After the arc surface correction, the reflection arc surface in the 3D display is corrected to a reflection plane. After the observation, it can be found that the horizontal extension of the crack top is long, the imaging amplitude value is large, the horizontal extension of the crack bottom is short, and the imaging amplitude value is low. The 3D display result after the arc surface correction is more convenient for observation and understanding.

The structure of the geological body near the well can be obtained by using the 3D display technology of reflection acoustic logging. After being processed by the arc correction technology, the geological body near the well can be more accurately depicted, which is more conducive to the application of reflection acoustic logging technology in petroleum geology.

Data Availability

All relevant data used to support the findings of this study are included within the article and also available from the corresponding author upon request.

Conflicts of Interest

The author declares that they have no conflicts of interest.

Acknowledgments

The logging data used in this paper are provided by the Acoustic Logging Laboratory of China University of Petroleum (Beijing), and we would like to express our thanks.

References

[1] J. L. Ben, W. X. Qiao, X. H. Che, X. D. Ju, J. Q. Lu, and B. Y. Men, "Experimental simulation of obtaining the reflector azimuth using azimuthal acoustic reflection tool in the underwater environment," *Journal of Petroleum Science and Engineering*, vol. 195, article 107649, 2020.

[2] X. Jiaqi, H. Hengshan, and Z. Wang, "Asymptotic solution to a 3D dipole single-well imaging system with combined monopole and dipole receivers with an application in elimination of azimuth ambiguity," *Geophysics*, vol. 84, no. 5, pp. D191–D207, 2019.

[3] J. Lai, G. Wang, Z. Fan et al., "Fracture detection in oil-based drilling mud using a combination of borehole image and sonic logs," *Journal of Petroleum Science and Engineering*, vol. 84, pp. 195–214, 2017.

[4] S. B. Yang, W. X. Qiao, X. H. Che, and X. Ju, "Numerical simulation of acoustic reflection logging while drilling based on a cylindrical phased array acoustic receiver station," *Journal of Petroleum Science and Engineering*, vol. 183, article 106467, 2019.

[5] S. B. Yang, W. X. Qiao, and X. H. Che, "Numerical simulation of acoustic fields in formation generated by linear phased array acoustic transmitters during logging while drilling," *Journal of Petroleum Science and Engineering*, vol. 182, article 106184, 2019.

[6] D. Li, W. Qiao, X. Che et al., "Eliminating the azimuth ambiguity in reflected S-wave imaging logging based on the azimuthal receiver mode," *Journal of Petroleum Science and Engineering*, vol. 199, article 108295, 2021.

[7] H. Gong, H. Chen, X. He, and X. Wang, "Eliminating the azimuth ambiguity in single-well imaging using 3C sonic data," *Geophysics*, vol. 80, no. 1, pp. A13–A17, 2015.

[8] K. Walker, J. Granville, and G. Kainer, "Towards the 3D measurement of formation properties in high-resolution with a continuous depth of investigation," in *SPE Annual Technical Conference and Exhibition*, Houston, TX, USA, 2015.

[9] Y. D. Zhang and H. S. Hu, "A technique to eliminate the azimuth ambiguity in single-well imaging," *Geophysics*, vol. 79, no. 6, pp. D409–D416, 2014.

[10] J. X. Li, K. A. Innanen, and G. Tao, "Extraction of reflected events from sonic-log waveforms using the Karhunen-Loève transform," *Geophysics*, vol. 82, no. 5, pp. D265–D277, 2017.

[11] T. Ling, S. Yan, Z. Zhigang et al., "Origin and evolution of overpressure in shale gas reservoirs of the Upper Ordovician Wufeng Formation–Lower Silurian Longmaxi Formation in the Sichuan basin," *Natural Gas Industry*, vol. 42, no. 10, pp. 48–64, 2022.

[12] H. Meng, X. Wang, H. Ge et al., "Balanced stress fracturing theory and its application in platform well fracturing during unconventional oil and gas development," *Energy Reports*, vol. 8, pp. 10705–10727, 2022.

[13] S. Han, C. Xiang, X. Du, L. Xie, S. Bai, and C. Wang, "Logging evaluation of deep multi-type unconventional gas reservoirs in the Songliao basin, Northeast China: implications from continental scientific drilling," *Geoscience Frontiers*, vol. 13, no. 6, article 101451, 2022.

[14] B. Lee and W. Rizkiningayu, "The importance of borehole image logs analysis in shale gas reservoirs development," in *The SPWLA 21st Formation Evaluation Symposium of Japan*, Chiba, Japan, 2015.

[15] C. H. Zuo, L. I. Honglei, L. I. Yingjie, S. H. Ziqi, and X. U. Guoqing, "The current status and development suggestions for shale oil reservoir stimulation at home and abroad," *Petroleum Drilling Techniques*, vol. 49, no. 4, pp. 1–7, 2021.

[16] L. Ma, H. Cao, Z. Zhang, Q. Gao, and Z. Luo, "An experimental investigation of the fracture behaviors of type-I cracks in shales with different bedding angles. Petroleum," *Science Bulletin*, vol. 4, pp. 347–353, 2019.

[17] J. Cai, L. Zhao, F. Zhang, and W. Wei, "Advances in multiscale rock physics for unconventional reservoirs," *Advances in Geo-Energy Research*, vol. 6, no. 4, pp. 271–275, 2022.

[18] B. E. Hornby, D. L. Johnson, K. W. Winkler, and R. A. Plumb, "Fracture evaluation using reflected Stoneley wave arrivals," *Geophysics*, vol. 54, no. 10, pp. 1274–1288, 1989.

[19] Y. Li, R. Zhou, X. Tang, J. C. Jackson, and D. J. Patterson, "Single-well imaging with acoustic reflection survey at mounds," in *Conference Proceedings, 64th EAGE Conference & Exhibition*, Mounds, OK, USA, 2002.

[20] X. M. Tang, "Imaging near-borehole structure using directional acoustic-wave measurement," *Geophysics*, vol. 69, no. 6, pp. 1378–1386, 2004.

[21] X. M. Tang and D. Patterson, "Single-well S-wave imaging using multicomponent dipole acoustic-log data," *Geophysics*, vol. 74, no. 6, pp. WCA211–WCA223, 2009.

[22] X. M. Tang, Y. Zheng, and D. J. Patterson, "Processing array acoustic logging data to image near-borehole geologic structures," *Geophysics*, vol. 72, no. 2, pp. E87–E97, 2007.

[23] X. M. Tang and Z. T. Wei, "Significant progress of acoustic logging technology: remote acoustic reflection imaging of a dipole acoustic system," *Applied Acoustics*, vol. 31, pp. 10–17, 2012.

[24] C. Li and W. Z. Yue, "High-resolution adaptive beamforming for borehole acoustic reflection imaging," *Geophysics*, vol. 80, no. 6, pp. D565–D574, 2015.

[25] C. Hei and Z. B. Xiao, "Borehole elastic wave anisotropic scattering and application to hydraulic fracturing," *Journal of Petroleum Science and Engineering*, vol. 183, article 106405, 2019.

[26] S. Q. Li, Y. D. Su, and X. M. Tang, "Research on a fast inversion method for structural strike around a borehole based on four-component dipole shear wave reflection imaging," *Chinese Journal of Geophysics*, vol. 63, no. 6, pp. 2478–2487, 2020.

[27] R. Kumar, N. Bennett, A. Donald, G. Martinez, and E. Velez, "3D borehole sonic imaging for input to structural modeling-a quantitative approach," in *SPE Middle East Oil and Gas Show and Conference*, Manama, Bahrain, 2019.

[28] Y. Karpekin, S. Orlova, and R. Tukhtaev, "Borehole acoustic reflection survey in horizontal wells: high resolution reservoir structure to guide properties distribution," in *SPE Russian Petroleum Technology Conference*, pp. 1–18, Moscow, Russia, 2019.